

Numerical Calculation of Effective Density and Compressibility Tensors in Periodic Porous Media: A Multi-Scale Asymptotic Method

Chang-Yong Lee¹, Michael J. Leamy^{*1}, and Jason H. Nadler²

School of Mechanical Engineering¹, Georgia Tech Research Institute (GTRI)²,
Georgia Institute of Technology, Atlanta, Georgia 30332

^{*}Michael J. Leamy: GWW School of Mechanical Engineering, 771 Ferst Drive N.W., Atlanta, GA 30332
michael.leamy@me.gatech.edu

Abstract: A major issue in predicting and controlling (via design) absorption properties of rigid porous media is the determination of the frequency-dependent effective density and compressibility tensors. Unlike previous research efforts which employ in-house and, oftentimes, multiple numerical procedures for determining these two essential tensors, we formulate their solution in terms of a set of micro-scale governing equations (and associated boundary conditions) resulting from a multi-scale asymptotic analysis. The form of these equations is ideally suited for incorporation into the finite element analysis package, COMSOL® Multiphysics. Incorporating the equations directly into COMSOL® allows for arbitrary three-dimensional model generation, unit cell meshing, and ultimate analysis using a single software package. We demonstrate the validity of this approach by comparing our numerical results with those published in the literature – specifically, we analyze porous media composed of rigid, face centered cubic (FCC) packed spheres.

Keywords: porous media, effective density, effective compressibility, acoustic absorption.

1. Introduction

Noise reduction is currently a major issue in the automobile, aeronautical, and building industries. One promising way to reduce noise is through the design and optimization of porous structures, which demonstrate favorable acoustic absorption properties due to fluid losses associated with large wetted areas. The important measurement parameters characterizing and predicting acoustic absorption performance of these structures are their effective density and compressibility tensors. For this reason, research attention devoted to the theoretical formulation of these two tensors has received considerable

attention in the past three decades¹⁻¹³. Although the formulations in the cited works are given in an explicit analytical form, they can only be evaluated in cases of very simple pore geometries assuming isotropic material properties, such as flow in a uniform cylinder. More recently, several numerical methods have been suggested in the literature¹⁴⁻²¹, which offer the possibility of extending the evaluation to general geometries and materials using desktop-based workstations. However, most of these analysis techniques require the use of (multiple) in-house codes and complicated numerical procedures. Furthermore, many of the cited numerical treatments are still not suitable for both arbitrary pore geometry and materials. Therefore, a need exists for a general computational approach for predicting the acoustic properties of periodic, porous materials which, ideally, can be cast in a form suitable for analysis using a commercial package, such as COMSOL® Multiphysics.

In this paper, we present a multi-scale numerical approach for determining the effective density and compressibility tensors for periodic porous media with arbitrary 3-D unit cells. To the authors' knowledge, the approach presented is the first posed in a consistent and general manner such that the resulting micro-scale equations can be implemented in a single commercial off-the-shelf (COTS) simulation code.

We begin by reviewing a mathematical procedure suitable for analyzing acoustic porous medium: the multi-scale asymptotic method (MAM)^{3,4,11,13}. MAM enables one to determine the macroscopic material description from knowledge of the physics and geometry at the microscopic level. We use this method to derive a set of frequency-domain partial differential equations, and boundary conditions, for coupled

dynamic and thermal response. COMSOL® Multiphysics is then employed with periodic boundary conditions on a unit fluid cell (UFC) to determine the effective density and compressibility tensors, which ultimately determine the acoustic absorption properties of the porous material. For a porous material composed of FCC packed spheres, comparisons of results generated in this study with those found in the literature^{15,17,18} demonstrate very good agreement.

2. Multi-Scale Asymptotic Method

In order to describe the linear acoustics phenomenon created in rigid porous medium, one has to solve the following set of harmonic viscothermal governing equations and associated boundary conditions for harmonic waves of frequency (f):

- In the viscothermal fluid flow,

$$\frac{P}{P_0} = \frac{\rho}{\rho_0} + \frac{\tau}{T_0} \quad (1)$$

$$\rho_0 i\omega \mathbf{u} = -\nabla p + (\lambda + \mu) \nabla(\nabla \cdot \mathbf{u}) + \mu \Delta \mathbf{u}$$

$$i\omega \frac{\rho}{\rho_0} = -\nabla \cdot \mathbf{u} \quad (2a,b)$$

$$\rho_0 i\omega C_p \tau = i\omega p + K \Delta \tau \quad (3)$$

- On the fluid-solid interface,

$$\mathbf{u} = 0 \text{ and } \tau = 0 \quad (4)$$

Eqs. (1-4) represent the equation of state, momentum balance, mass balance, and energy balance. P_0 , ρ_0 , and T_0 denote the pressure, density, and temperature of the air at rest, while \mathbf{u} , p , ρ , and τ the fluid velocity, pressure variation, density variation, and temperature variation. In addition, the angular frequency, shear and bulk viscosities, specific heat at constant pressure, and heat conductivity are denoted, respectively, by $\omega (=2\pi f)$, μ , λ , C_p , and K . As has been noted by several authors, any problem of linear acoustics involving porous medium can be dealt with using this formalism. However, because the equations presented above are based on interdependent macroscopic variables, they cannot take into account explicitly the micro-scale physics and geometry of the porous media at the microscopic level.

MAM is a multi-scale approach based on an asymptotic analysis of the governing equations (1-4). It is used to further derive a set of well-posed micro-scale equations necessary for computing effective macro-scale variables, via averaging. The asymptotic approach begins by introducing two space variables: x for the macro-variations and $y = \varepsilon^{-1}x$ for the micro-variations. Here the small parameter $\varepsilon = O(l/L) \ll 1$ is a scale ratio of a characteristic unit cell length l and frequency-dependent wavelength L . As such, the small parameter denotes a ratio of a micro-scale characteristic length to a macro-scale characteristic length. The solution variables sought and the differential operators are next split into their macroscopic and microscopic components via power series involving ε ,

$$\begin{aligned} \mathbf{u} &= \mathbf{u}^0(x, y) + \varepsilon \mathbf{u}^1(x, y) + \varepsilon^2 \mathbf{u}^2(x, y) + \dots \\ p &= p^0(x, y) + \varepsilon p^1(x, y) + \varepsilon^2 p^2(x, y) + \dots \\ \tau &= \tau^0(x, y) + \varepsilon \tau^1(x, y) + \varepsilon^2 \tau^2(x, y) + \dots \end{aligned} \quad (5)$$

The gradient (∇) and Laplacian (Δ) operators take the forms,

$$\nabla = \nabla_x + \frac{1}{\varepsilon} \nabla_y \text{ and } \Delta = \Delta_x + \frac{2}{\varepsilon} \Delta_{xy} + \frac{1}{\varepsilon^2} \Delta_y. \quad (6)$$

Moreover, because one can consider the viscothermal effects to occur at the micro-scale, it is necessary to rescale the viscosity and conductivity coefficients appearing in the momentum balance (2a) and energy equations (3) by ε^2 ¹¹

$$\rho_0 i\omega \mathbf{u} = -\nabla p + \varepsilon^2 [(\lambda + \mu) \nabla(\nabla \cdot \mathbf{u}) + \mu \Delta \mathbf{u}] \quad (7)$$

$$\rho_0 i\omega C_p \tau = i\omega p + \varepsilon^2 [K \Delta \tau] \quad (8)$$

With this rescaling, MAM allows for orderly solution of the seeking variables.

We start with the mass balance equation (2b), combined with the state equation (1). Updated using the expansions (5-6), a single multi-scaled relationship results,

$$\begin{aligned} i\omega \left[\frac{(p^0 + \varepsilon p^1 + \dots)}{P_0} - \frac{(\tau^0 + \varepsilon \tau^1 + \dots)}{T_0} \right] \\ = - \left(\nabla_x + \frac{1}{\varepsilon} \nabla_y \right) \cdot (\mathbf{u}^0 + \varepsilon \mathbf{u}^1 + \dots) \end{aligned} \quad (9)$$

Separating scales, the corresponding equation at the highest order ε^{-1} implies that the fluid velocity can be considered as locally incompressible,

$$\nabla_y \cdot \mathbf{u}^0 = 0, \quad (10)$$

while at order ε^0 ,

$$i\omega \left[\frac{p^0}{P_0} - \frac{\tau^0}{T_0} \right] = -\nabla_x \cdot \mathbf{u}^0. \quad (11)$$

A similar procedure carried-out on the momentum balance equation (7) yields:

$$\begin{aligned} \rho_0 i\omega (\mathbf{u}^0 + \varepsilon \mathbf{u}^1 + \dots) &= -\left(\nabla_x + \frac{1}{\varepsilon} \nabla_y \right) (p^0 + \varepsilon p^1 + \dots) \\ &+ \varepsilon^2 \left\{ \mu \left(\Delta_x + \frac{2}{\varepsilon} \Delta_{xy} + \frac{1}{\varepsilon^2} \Delta_y \right) (\mathbf{u}^0 + \varepsilon \mathbf{u}^1 + \dots) \right. \\ &\left. + (\lambda + \mu) \left(\nabla_x + \frac{1}{\varepsilon} \nabla_y \right) \left(\left(\nabla_x + \frac{1}{\varepsilon} \nabla_y \right) \cdot (\mathbf{u}^0 + \varepsilon \mathbf{u}^1 + \dots) \right) \right\} \end{aligned} \quad (12)$$

Separating orders, order ε^{-1} yields the relationship,

$$\nabla_y p^0 = 0 \Rightarrow p^0(x, y) = p^0(x) \quad (13)$$

which implies that the macro-scale pressure is constant at the micro-scale. At order ε^0 ,

$$\rho_0 i\omega \mathbf{u}^0 = -\nabla_y p^1 - \nabla_x p^0 + \mu \Delta_y \mathbf{u}^0. \quad (14)$$

For the energy equation (8), the procedure results in the multi-scale equation,

$$\begin{aligned} \rho_0 i\omega C_p (\tau^0 + \varepsilon \tau^1 + \dots) &= i\omega (p^0 + \varepsilon p^1 + \dots) \\ &+ \varepsilon^2 \left[K \left(\Delta_x + \frac{2}{\varepsilon} \Delta_{xy} + \frac{1}{\varepsilon^2} \Delta_y \right) (\tau^0 + \varepsilon \tau^1 + \dots) \right] \end{aligned} \quad (15)$$

The highest order identified is ε^0 and thus a single relationship is obtained (macro-scale),

$$\rho_0 i\omega C_p \tau^0 = i\omega p^0 + K \Delta_y \tau^0. \quad (16)$$

Following the methodology introduced by Lafarge et al¹⁰, we assume, at a given frequency, the appropriate solution forms of the macro-scale velocity (\mathbf{u}^0) and micro-scale pressure (p^1) distributions as linear relationships with $\nabla_x p^0$, while the macro-scale temperature (τ^0) distribution as linearly-related to $i\omega p^0$, as follows:

$$\begin{aligned} \mathbf{u}^0(x, y) &= -\frac{\mathbf{k}_j(y, \omega)}{\mu} \nabla_x p^0(x), \quad j=1,2,3 \\ p^1(x, y) &= \mathbf{a}(y, \omega) \cdot \nabla_x p^0(x) + \hat{p}^1(x) \end{aligned} \quad (17)$$

and

$$\tau^0(x, y) = \frac{k'(y, \omega)}{K} i\omega p^0(x) \quad (18)$$

Note that \mathbf{k}_j and k' denote the dynamic viscous and thermal permeability, and also note that the pressure (p^1) can be expressed in terms of its deviatoric part (\hat{p}^1) and zero mean value (\mathbf{a}) on the UFC. Substituting (17-18) into (10), (14),

and (16) yields the following decoupled set of partial differential equations suitable for incorporation into COMSOL® Multiphysics:

- Momentum equation with no-slip boundaries

$$\begin{aligned} i\omega \frac{\rho_0}{\mu} \mathbf{k}_j \cdot \mathbf{e} - \nabla \cdot \mathbf{a} \cdot \mathbf{e} - \Delta \mathbf{k}_j \cdot \mathbf{e} &= \mathbf{e} \\ \nabla \cdot \mathbf{k}_j \cdot \mathbf{e} &= 0 \text{ in } \Omega_f \end{aligned} \quad (19)$$

$\mathbf{k}_j = 0$ on Γ , \mathbf{k}_j & \mathbf{a} : Ω -periodic

where \mathbf{e} denotes any of three unit vectors directed along a global coordinate system.

- Energy equation with isothermal boundaries

$$\frac{\rho_0 \text{Pr}}{\mu} i\omega \rho_0 k' - \Delta k' = -1 \text{ in } \Omega_f \quad (20)$$

$k' = 0$ on Γ , k' : Ω -periodic,

where $\text{Pr} = \mu C_p / K$ denotes the Prandtl number.

Here Ω , Ω_f and Γ represent the UFC volume, the fluid-filled pore volume, and the fluid-solid interface, respectively. Taking the volume average of Eqs. (11), (17) and (18) over the UFC and using the relationship between the effective (χ_{eff}) and dynamic (β) compressibilities,

$$\frac{\beta(\omega)}{\gamma P_0} i\omega \langle p^0 \rangle = -\nabla_x \cdot \langle \mathbf{u}^0 \rangle, \text{ with } \chi_{\text{eff}} = \frac{\beta(\omega)}{\gamma P_0} \quad (21)$$

which is defined by Lafarge⁹, yields two macroscopic equations as follows:

$$\begin{aligned} \mathbf{p}_{\text{eff},j} i\omega \langle \mathbf{u}^0 \rangle &= -\nabla_x \langle p^0 \rangle, \\ \chi_{\text{eff}} i\omega \langle p^0 \rangle &= -\nabla_x \cdot \langle \mathbf{u}^0 \rangle, \end{aligned} \quad (22)$$

where

$$\begin{aligned} \mathbf{p}_{\text{eff},j} &= \frac{\mu \phi}{i\omega} \hat{\mathbf{k}}_j \\ \chi_{\text{eff}} &= \frac{\beta(\omega)}{\gamma P_0} = \frac{1}{\gamma P_0} \left[\gamma - (\gamma - 1) \frac{\rho_0 \text{Pr}}{\mu} \frac{i\omega \hat{k}'}{\phi} \right] \end{aligned} \quad (23)$$

with γ as the specific heat ratio, $\langle \bullet \rangle = \frac{1}{\Omega_f} \int_{\Omega} \bullet d\Omega$,

$\phi = \frac{\Omega_f}{\Omega}$, $\hat{\mathbf{k}}_j = \phi \langle \mathbf{k}_j \rangle$, and $\hat{k}' = \phi \langle k' \rangle$. Here, $\mathbf{p}_{\text{eff},j}$ and χ_{eff} are identified as the effective density and compressibility tensors, which ultimately dictate the medium's acoustic absorption behavior.

3. Numerical Implementation in COMSOL

To assess the validity of the described MAM process and numerical implementation, we calculated effective tensors for the FCC geometry^{17,18} depicted in Fig. 1 subject to mirror symmetry (y - and z -directions) and translational periodicity (x -direction) boundary conditions. This figure depicts an irreducible unit cell consisting of a fluid-filled interstitial space between FCC packed spheres.

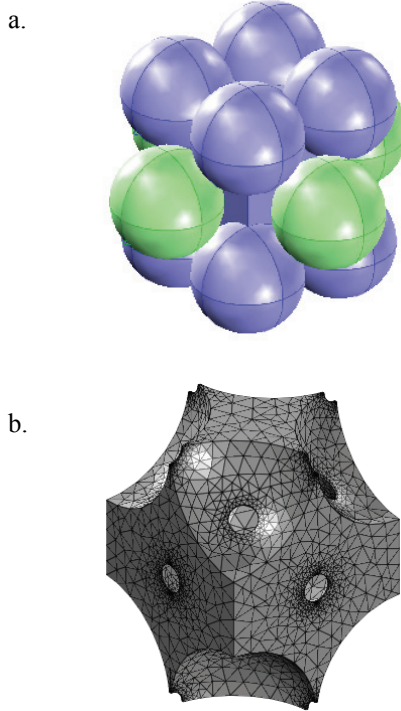


Figure 1 (a) original FCC structure (b) corresponding meshed FCC UFC in COMSOL multiphysics.

Using COMSOL® Multiphysics, the numerical solutions of the dynamic viscous and heat equations are calculated from Eqs. (19) and (20). Table 1 provides the coefficients used to arrive at the numerical solutions.

Table 1 Coefficients for a FCC stacking of beads.

ρ_0	T_0	P_0	μ	Pr	γ
1.293 [kgm ⁻³]	300 [K]	10^5 [Pa]	1.7210^{-5} [kg(ms) ⁻¹]	0.715	1.4

To directly compare our numerical results with those presented in the literature^{17,18}, the radius of the sphere is chosen as 1 mm. As in the cited studies, we also include a soldering neck at each

sphere contact point, where the solder radius used is 150 μm .

4. Results and Discussion

For a given frequency, using COMSOL® Multiphysics we obtain numerical results for the macro-scale velocity and temperature distributions within an irreducible UFC. We present results where we restrict the unit vector \mathbf{e} to the x -axis. Fig. 2 provides an example dynamic and thermal permeability distribution at 500 Hz in a y - z plane.

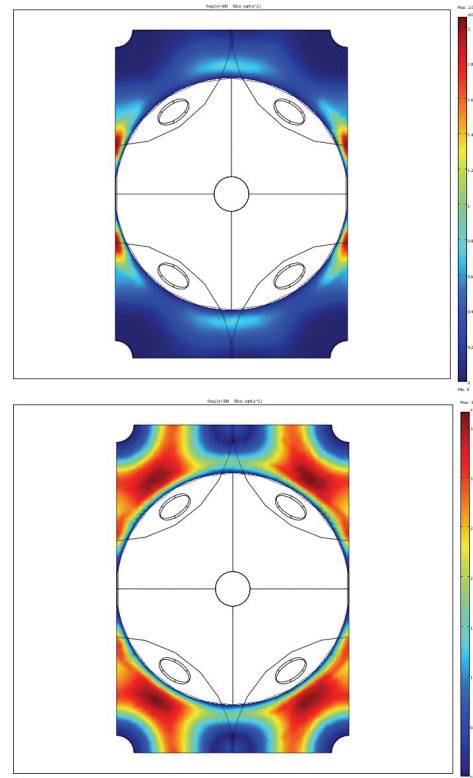


Figure 2 Magnitude of dynamic (top) and heat (bottom) permeability distributions at 500 Hz.

We then employ a COMSOL® script to iteratively compute the effective density and compressibility tensors (23) in a frequency range of interest (here, from 10 to 10,000 Hz). The results are presented in Fig. 3. For validation purposes, numerical points provided in the literature¹⁸ are also plotted. As can be seen in the subfigures, the frequency-dependent effective tensors obtained from our approach are in very

good agreement with those provided by Ref. 18 over the entire range of frequencies considered.

Moreover, as additional outcomes of the numerical procedure, the porosity (ϕ), the static viscous permeability and tortuosity (k_0, α_0), the tortuosity (α_∞), the static thermal permeability and tortuosity (k'_0, α'_0), and the viscous and thermal characteristic lengths (Λ, Λ') are automatically computed. These parameters provide an alternative, analytic-based means to calculate the effective density and compressibility tensors^{19,20,21}. The results are gathered in Table 2 for comparison with those available in the literature^{15,17,18}.

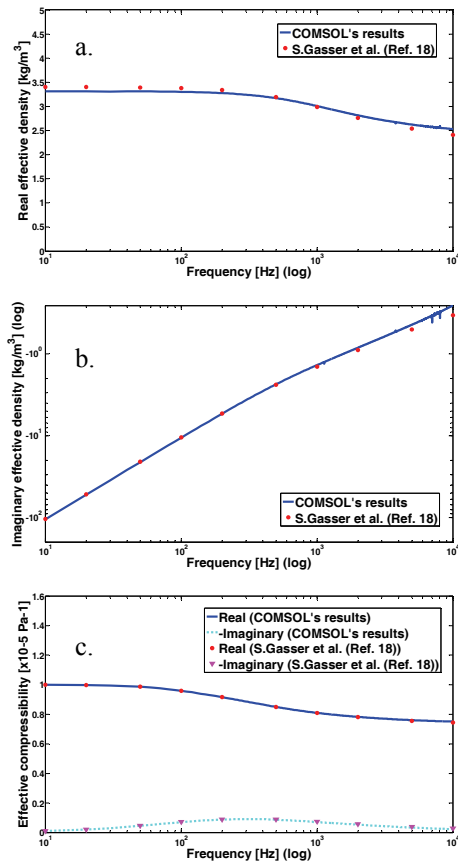


Figure 3 (a) real and (b) imaginary parts of the effective density via frequency (c) effective compressibility via frequency.

Table 2 shows good agreement between published results and our numerical results. However, as concerns the viscous characteristic length, there are disagreements with three numerical values. As mentioned in Ref. 17, this can be explained by the

presence of soldering necks. Also, the static viscous tortuosity is 14 % lower than the value obtained in this study. A possible explanation for this disagreement is the use of a different definition used to calculate the value – values obtained from Refs. 17 and 18 were indirectly calculated using a very low frequency (10⁻³ Hz), whereas our approach was directly estimated according to Ref. 20,

$$\alpha_0 = \langle \mathbf{k}_{0j}^2 \rangle / \langle \mathbf{k}_{0j} \rangle^2. \quad (23)$$

Table 2 Computations of the acoustic properties of a FCC sphere stacking versus those available in the literature.

	Ref. 15	Refs. 17, 18	COMSOL
ϕ	0.26	0.26	0.26
k_0	$6.95 \cdot 10^{-10}$	$6.83 \cdot 10^{-10}$	$6.73 \cdot 10^{-10}$
α_0	NA	2.63	2.24
α_∞	1.61	1.66	1.65
k'_0	NA	$0.274 \cdot 10^{-10}$	$0.272 \cdot 10^{-10}$
α'_0	NA	1.85	1.87
Λ	$0.124 \cdot 10^{-3}$	$0.164 \cdot 10^{-3}$	$0.173 \cdot 10^{-3}$
Λ'	NA	$0.249 \cdot 10^{-3}$	$0.247 \cdot 10^{-3}$

5. Conclusions

In conclusion, we present a consistent and general approach for numerically computing frequency-dependent effective density and compressibility tensors for periodic porous materials. These tensors ultimately characterize the acoustic absorption behavior of the material. The formulation is cast in a form suitable for incorporation into COMSOL® Multiphysics, and as such, avoids the complication of working with and coupling multiple in-house codes, as done in previous investigations. Comparisons of results generated in this study with published numerical data demonstrate very good agreement over all frequencies considered.

6. References

1. G. Kirchhoff, "Über den einfluß der wärmeleitung in einem gase auf die schallbewegung," *Ann. Phys. Chem.* **134**, 177 (1868).
2. M. A. Biot, "Theory of propagation of elastic waves in a fluid saturated porous solid II: Higher

- frequency range,” *J. Acoustic. Soc. Am.* **28**, 179 (1956).
3. J. L. Auriault, “Dynamic behaviour of a porous media saturated by a Newtonian fluid,” *Int. J. Engng. Sci.* **18**, 775 (1980)
 4. J. L. Auriault, L. Borne, and R. Chambon, “Dynamics of porous saturated media, checking of the generalized law of Darcy,” *J. Acoust. Soc. Am.* **77**, 1641 (1985)
 5. D. L. Johnson, J. Koplik, and R. Dashen, “Theory of dynamic permeability and tortuosity in fluid-saturated porous media,” *J. Fluid Mech.* **176**, 379 (1987).
 6. Y. Champoux and J. F. Allard, “Dynamic tortuosity and bulk modulus in air-saturated porous media,” *J. Appl. Phys.* **70**, 1975 (1991).
 7. J. F. Allard, *Propagation of Sound in Porous Media*, Elsevier Applied Science, Amsterdam, 1993.
 8. S. R. Pride, F. D. Morgan, and A. F. Gangi, “Drag forces of porous medium acoustics,” *Phys. Rev. B* **47**, 4964 (1993).
 9. D. Lafarge, “Propagation du son dans les matériaux poreux à structure rigide saturés par un fluide viscothermique,” Ph.D. thesis, Université du Maine, 1993.
 10. D. Lafarge, P. Lemarinier, and J. F. Allard, “Dynamic compressibility of air in porous structures at audible frequencies,” *J. Acoust. Soc. Am.* **102**, 1995 (1997).
 11. C. Boutin, P. Royer, and J. L. Auriault, “Acoustic absorption of porous surfacing with dual porosity,” *Int. J. Solids Struct.* **35**, 4709 (1998).
 12. J. G. Berryman, “Comparison of upscaling methods in poroelasticity and its generalizations,” *J. Eng. Mech.* **131**, 928 (2005).
 13. C. Boutin, “Rayleigh scattering of acoustic waves in rigid porous media,” *J. Acoustic. Soc. Am.* **122**, 1888 (2007).
 14. M. Y. Zhou and P. Sheng, “First-principles calculations of dynamic permeability in porous media,” *Phys. Rev. B* **39**, 12027 (1989).
 15. A. M. Chapman and J. J. L. Higdon, “Oscillatory Stokes flow in periodic porous media,” *Phys. Fluids A* **4**, 2099 (1992).
 16. L. Borne, “Harmonic Stokes flow through periodic porous media: a 3D boundary element method,” *J. Comput. Phys.* **99**, 214 (1992).
 17. S. Gasser, “Etude des propriétés acoustiques et mécaniques d’un matériau métallique poreux modèle à base de sphères creuses de nickel,” Ph.D. thesis, ONERA, (2003).
 18. S. Gasser, F. Paun, and Y. Bréchet, “Absorptive properties of rigid porous media: Application to face centered cubic sphere packing,” *J. Acoust. Soc. Am.* **117**, 2090 (2005).
 19. K. Schladitz, S. Peters, D. Reinel-Bitzer, A. Wiegmann, and J. Ohser, “Design of acoustic trim based on geometric modeling and flow simulation for non-woven,” *Comput. Mater. Sci.* **38**, 56 (2006).
 20. C. Perrot, F. Chevillotte, and R. Panneton, “Dynamic viscous permeability of an open-cell aluminum foam: computations versus experiments,” *J. Acoust. Soc. Am.* **103**, 024909 (2008).
 21. C. Perrot, F. Chevillotte, and R. Panneton, “Bottom-up approach for microstructure optimization of sound absorbing materials,” *J. Acoust. Soc. Am.* **124**, 940 (2008).

7. Acknowledgements

The authors gratefully acknowledge the EADS N.A. Foundation’s support of this work.